Available online at www.sciencedirect.com
ScienceDirect
Thermochimica Acta 461 (2007) 137–144
thermochimica acta
www.elsevier.com/locate/tca

Effect of water on the thermal properties of silk fibroin

Xiao Hu [a], David Kaplan [b], Peggy Cebe [a,*]

[a] Department of Physics and Astronomy, Tufts University STC-208, 4 Colby Street, Medford, MA 02155, United States
[b] Departments of Biomedical Engineering and Chemical and Biological Engineering, Tufts University, Medford, MA 02155, United States

Available online 14 December 2006

Abstract

Silk fibroin films cast from water solution, and containing bound water, are quantitatively studied in this work. First, to obtain the solid and liquid heat capacities of the pure dry silk fibroin, cyclic heat treatment was used to monitor the process of removing the bound water. After water removal, the glass transition of pure non-crystalline silk was observed at 451 K (178 °C). The solid and liquid heat capacities of the pure silk fibroin were then measured using differential scanning calorimetry (DSC), temperature-modulated DSC (TMDSC), and quasi-isothermal TMDSC, and found to be: $C_p(T)^{\text{solid}} = 0.134 + 3.696 \times 10^{-3}\,T$ J/g K and $C_p(T)^{\text{liquid}} = 0.710 + 3.47 \times 10^{-3}\,T$ J/g K over the temperature region from 200 to 450 K. These heat capacities were used to construct the underlying baseline heat capacity for the combined silk–water system.

When the combined silk–water system is studied, bound water is lost from the film during heating, and the loss of mass is quantified using thermogravimetric analysis (TGA). Bound water in the silk film acts as a plasticizer, and a lower glass transition of the silk–water system is observed. Comparison of the measured heat capacity of the silk–water system to the calculated total baselines was made in the vicinity of the water-induced glass transition. Results show that the total solid specific heat capacity is in good agreement with the calculated solid baseline in the low-temperature region below about 240 K. As temperature increases above the lower glass transition, all bound water eventually leaves the silk, and the free volume and the silk mobility are reduced. This allows the upper glass transition of the dried silk to be observed.

Keywords: *Bombyx mori* silk fibroin; Heat capacity; DSC; Bound water; Glass transition

1. Introduction

Domesticated (*Bombyx mori*) silk worm fiber has been studied for many years [1,2]. The filament of the silk fiber, silk fibroin, is coated with a water-soluble protein glue, sericin, to form the natural silk fiber. As the interior structural protein of silk fiber, silk fibroin has been used in many fields including biomaterials applications [3,4]. In the gland of *B. mori* silkworms, the water-soluble silk fibroin solution and the sericin are spun together into a fiber, leading to a new insoluble conformation due to a rapid change in structure of the fibroin. The sericin is added to the surface of silk fibroin during spinning, and the result is the formation of the silk fiber.

The phase transitions of silk fibroin have been well studied and were a result of the formation of anti-parallel beta-sheet structure. Exposure of the aqueous solution of fibroin to organic solvents, mechanical stress and thermal treatment can induce formation of the insoluble beta-sheet structure in degummed silk fibroin films [2,5–11]. However, the mechanism of beta-sheet-crystallization is still unclear. One reason for this uncertainty is that silk fibroin crystallizes rapidly, making the initial stages of crystallization difficult to study. We have used thermal analysis and infrared spectroscopy to determine the content of beta sheet after thermal crystallization [10,11]. Thermal crystallization provides a wide temperature region to study the structural transitions of the silk fibroin because of the high glass transition temperature, T_g = 451 K (178 °C) of this protein. In addition, its isothermal crystallization above T_g is much slower than in the natural spinning process [10,11].

In the present work, we investigate the impact of water on the thermal properties of silk fibroin. Water in polymeric systems can be classified into three types [12–14]: freezing free water, freezing bound water, and non-freezing bound water. According to McGrath and co-workers [13], freezing free water in polymers is unbound water that has the same transition temperature at 273 K as bulk water. In our silk–water system, the freezing free water can be removed by keeping the samples in a vacuum oven for several days. Freezing bound water is attributed to the weak interaction between water and polymer and will also undergo the freezing transition. Non-freezing bound water results from

* Corresponding author. Tel.: +1 617 627 3365; fax: +1 617 627 3744.
E-mail address: peggy.cebe@tufts.edu (P. Cebe).

0040-6031/$ – see front matter © 2007 Elsevier B.V. All rights reserved.
doi:10.1016/j.tca.2006.12.011

strong interaction between the polymer and water. McGrath and co-workers [13] found that the non-freezing strongly bound water acts as a plasticizer in polymeric systems while freezable water did not affect the polymer T_g. The sum of the freezing bound and non-freezing bound water fractions is the bound water content. The bound water content depends on the chemical structure and on the higher-order structure of the polymer. In our study the major water influence comes from freezing free water, which is always removed prior to our investigations, and bound water which is the subject of the present study. The bound water in the glassy state is termed "glassy" water following the language of Pyda [16,17] which implies amorphous, non-crystalline water of low mobility.

Recent study showed that silk films cast from water solution contained intermolecularly bound water molecules that could plasticize the silk, causing a reduction of the glass transition temperature [8,14]. Rapid heating of the samples containing water allows the non-freezing bound water to remain inside the film temporarily, thus lowering T_g [8]. By controlling the humidity during preparation of the silk fibroin samples, the glass transition can be adjusted to different temperatures. In a study of the early stages of solution crystallization of silk fibroin, we have previously pointed out that water makes important contributions to the crystallization process of the spun fiber [15]. Therefore, it is necessary to study in detail the water-induced glass transition of plasticized silk fibroin, and to determine the relationship between the reduction in T_g and the formation of beta-sheet crystalline structures. The results of this study will have impact on our understanding of the crystallization kinetics of plasticized silk, bearing directly on the process wherein water-soluble silk fibroin is transformed into insoluble silk fibroin containing beta-sheet crystals.

Pyda et al. recently reported a method and process to study thermal interactions between polymers and small molecules, using the starch–water system as a model [16–18]. This contribution provides a useful roadmap to study water-induced glass transitions for silk fibroin. Thus, this approach was followed in the present study in order to determine the effects of water on the specific heat capacity of silk fibroin. Traditional differential scanning calorimetry (DSC) and a temperature-modulated variant of this technique (TMDSC), as well as quasi-isothermal TMDSC, were used to explore silk fibroin–water interactions.

2. Experimental

2.1. Materials and preparation

Cocoons of *B. mori* silkworm silk (obtained from Tsukuba, Japan) were boiled for 25 min in an aqueous solution of 0.02 M Na_2CO_3 and rinsed thoroughly with water to extract the glue-like sericin [2]. The remaining silk fibroin was dissolved in a 9.3 M LiBr solution at 333 K (60 °C) for 4–6 h and then dialyzed in distilled water using a Slide-a-Lyzer dialysis cassette (Pierce, MWCO 3500) for 2 days. After centrifugation and filtration to remove insoluble residues, the final 2 wt% silk fibroin aqueous solution was cast in polystyrene Petri dishes to make silk fibroin films. The fibroin films were then put into a vacuum oven at room temperature for 1 day to remove moisture on their surfaces. Immediately after casting, and prior to any crystallization procedure, the films were completely non-crystalline and there was no signature of beta-pleated sheets in either the FTIR absorption spectrum or the WAXS diffractogram. Detailed verification of this process was reported in our previous work [10].

2.2. Differential scanning calorimetry

Samples with of about 8 mg were encapsulated in Al pans and heated in a TA Instruments Q100 DSC, which was purged with a dry nitrogen gas flow of 50 mL/min. The instrument was calibrated for empty cell baseline, and with indium for heat flow and temperature. Standard mode DSC measurements were performed at a heating rate of 2 K/min (for pure silk fibroin). Temperature-modulated differential scanning calorimetry (TMDSC) measurements were also performed using a TA Instruments Q100, equipped with a refrigerated cooling system. The less ordered (non-crystalline) samples were heated at 2 K/min with a modulation period of 60 s and temperature amplitude of 0.318 K. The silk–water system was heated at 5 K/min with a period of 40 s and temperature amplitude of 0.5 K. Aluminum and sapphire reference standards were used for calibration of the heat capacity. TMDSC endotherms are presented with downward deflection from the baseline. The heat capacity measurement consisted of three runs, as described in our earlier work [10]. The first run is empty Al sample pan versus empty Al reference pan to obtain the cell asymmetry and baseline correction. The second run is sapphire standard versus empty Al reference pan to calibrate heat flow amplitude according to standard equations, published previously [10,19–24]. The third run is sample versus empty Al reference pan. The same empty Al reference pan was used in all the runs, and all the Al sample pans were kept the same in weight. From a standard DSC measurement with a constant applied heating rate we obtain the total heat capacity, which consists of both the reversing and non-reversing components, from

$$mC_p = K'' \frac{\mathrm{HF}}{q} \tag{1}$$

where K'' is a calibration constant, and HF is the heat flow.

In TMDSC we measure the "reversing heat capacity", a term defined in TMDSC to represent a heat effect, which can be reversed within the temperature range of the modulation and calculated from [19–21,24,25]:

$$|mC_p + C_\mathrm{s} - C_\mathrm{r} \pm \Delta C_\mathrm{cell}| = \left(\frac{A_T}{A}\right)\left[\left(\frac{K}{\omega}\right)^2 C_\mathrm{r}^2\right]^{1/2} \tag{2a}$$

$$|mC_p + C_\mathrm{s} - C_\mathrm{r} \pm \Delta C_\mathrm{cell}| = K' \frac{A_\mathrm{HF}}{A} \tag{2b}$$

where mC_p is the heat capacity of a sample of mass, m, and specific heat capacity, C_p, C_s the heat capacity of the sample pan, C_r the heat capacity of an empty reference pan, and ΔC_cell is the cell asymmetry correction which can be determined by running

a series of empty pans with various mass differences compared to the reference [20,21]. On the right hand side of Eq. (2), A_T is the amplitude of temperature difference between sample and reference, A the sample temperature modulation amplitude, K the Newton's law calibration constant which is independent of modulation frequency and reference, A_{Hf} the heat flow amplitude and K' is a calibration constant at each individual temperature provided the same experimental conditions are maintained to assure the same heat transfer (e.g., same reference, same modulation frequency).

The quasi-isothermal TMDSC procedure was carried out over the temperature range of 413–473 K with a stepwise temperature increase of 2 K. The temperature modulation amplitude is 0.5 K, and the oscillation period is 1 min. Each quasi-isothermal run lasted 20 min per temperature step, and the heat capacity at given T_0 was calculated by averaging the data points collected during the last 10 min. Plotting the Lissajous figures of modulated heat flow versus modulated temperature was used to check the establishment of steady state. A perfect ellipse always appeared when steady state is reached, as occurred during the last 10 min of the quasi-isothermal step.

2.3. Thermal gravimetric analysis

Thermal gravimetric analysis (TGA, TA Instruments Q500) was used to measure changes in weight of silk fibroin samples with increasing temperature. TGA curves were obtained under nitrogen atmosphere with a gas flow of 50 mL/min. The experiments were performed at heating rates of 2, 5, 10, and 20 K/min.

3. Results and discussion

3.1. Thermal cycling studies

It has been reported that water molecules inside silk fibroin films can induce a low-temperature glass transition during the rapid heating process [8]. With an increase of the water content in the silk film, the temperature value of this water-induced glass transition decreased gradually. Therefore, in the process of measuring the heat capacity of pure silk fibroin, we had to avoid the formation of this water-induced glass transition. In our previous work [10], the effect of the water-induced glass transition could be reduced by using a slow heating process (~2 K/min), with the added condition that the sample had been put into a vacuum oven for 3–4 days to remove the moisture and the freezing free water.

Fig. 1a and b shows the TMDSC non-reversing (NR), and reversing (R), heat flows, respectively, during a thermal cycling study, using six cycles of a heat–cool–reheat process to monitor the change of heat flow during water removal at heating/cooling rates of ±2 K/min. The six cycles take the film to steadily increasing temperatures (T_{end} = 338 K, 368 K, 398 K, 428 K, 458 K, and 483 K). Only the heating traces are shown in Fig. 1.

In the first heating process (curve 1), silk fibroin was heated from just above room temperature (308 K) to 338 K, and then it was cooled to 308 K. During this process, some intermolecular

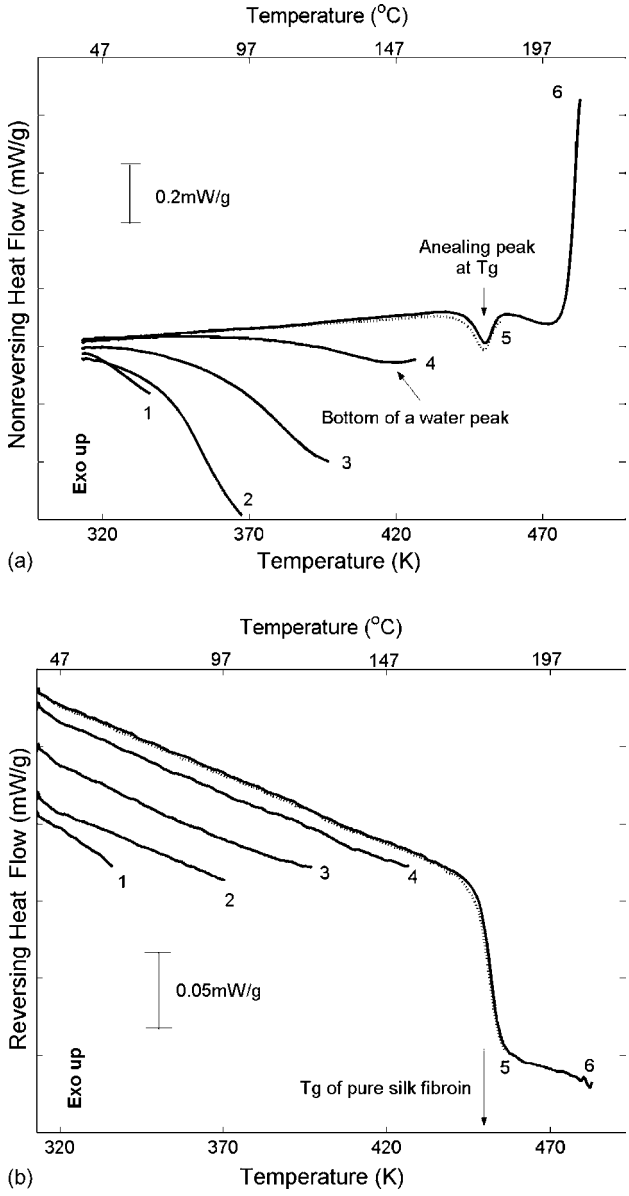

Fig. 1. TMDSC normalized non-reversing (a) and reversing (b) heat flow vs. temperature during a thermal cycling study. Six cycles (curves 1–6) of a heat–cool–reheat process were used to monitor the change of heat flow during water removal, at heating/cooling rates of ±2 K/min. Only the heating traces are shown. The arrow marks the temperature of the pure silk without water.

bound water was evaporated resulting in a mass decrease in the sample. The NR heat flows (Fig. 1a, curves 1–4) show a curved trace of bound water lost through the first four cycles, while the R heat flow is nearly linear with temperature increase during these cycles.

As the mass of the sample is reduced with the progressive evaporation of bound water, each of the mass-normalized (mW/g) reversing heat flow traces is higher than the previous one. A straight line in the R heat flow indicates that there is no glass transition occurring during the first four heating cycles. Finally, the R heat flow reached the glass transition of the pure silk fibroin (T_g = 451 K [1,2,10]) in cycle 5 (T_{end} = 458 K). When it touched the ending temperature of 458 K, the heater went back

immediately to 308 K. The sample was then heated again to the final ending temperature of 483 K, which is shown in curve 6. The NR and R traces of 5 and 6 totally overlapped each other. This result indicates that: (1) there is no more water in the film during cycles 5 and 6; (2) from cycles 1 to 5, water molecules inside the silk fibroin are completely removed, as can be seen by monitoring the mass lost which affects the specific R heat flow curve; (3) no additional glass transition occurs at a temperature lower than the temperature of pure silk fibroin (T_g = 451 K). Therefore, pure silk fibroin made through this cyclic procedure is free of water, and if we measured the exact mass at this time, the specific heat capacity of pure silk fibroin can be obtained accurately.

3.2. Heat capacity of pure silk fibroin

The heat capacity of the pure silk fibroin was measured by TMDSC. In our previous work [1,2,10], we demonstrated that room-temperature cast silk fibroin films are non-crystalline, even for thin samples cast from a low concentration solution (<5% silk in water). The glass transition is near 451 K and the average value for heat capacity increment at T_g of less ordered silk fibroin was determined to be $\Delta C_{p_0}(T_g) = 0.478 \pm 0.005$ J/g K. In the present study, the intermolecular bound water in the silk fibroin film was carefully removed by a cyclic process as described above, and a wider region of the TMDSC scan (213 K to 573 K) was performed on the treated samples compared with our previous work [10].

Fig. 2 shows the TMDSC total heat flow (upper curve), and reversing heat flow (lower curve) of a less ordered, non-crystalline film from 213 to 548 K. The tiny endothermic peak in the total heat flow signal (downward deflection from the baseline) at the location of the glass transition is due to the physical relaxation caused by the cyclic heating and cooling procedures for removing the intermolecular water in the silk fibroin film. This small peak does not affect the step height of the R heat flow (lower curve) at T_g. Above the temperature of the glass transition step, the total heat flow shows a large exothermic peak centered at about 485 K from beta sheets crystallizing non-isothermally during the scan, and there is onset of thermal degradation at higher temperature, which can be seen as a large endothermic peak centered at about 536 K. No melting endothermic can be observed in the silk fibroin sample due to the onset of degradation.

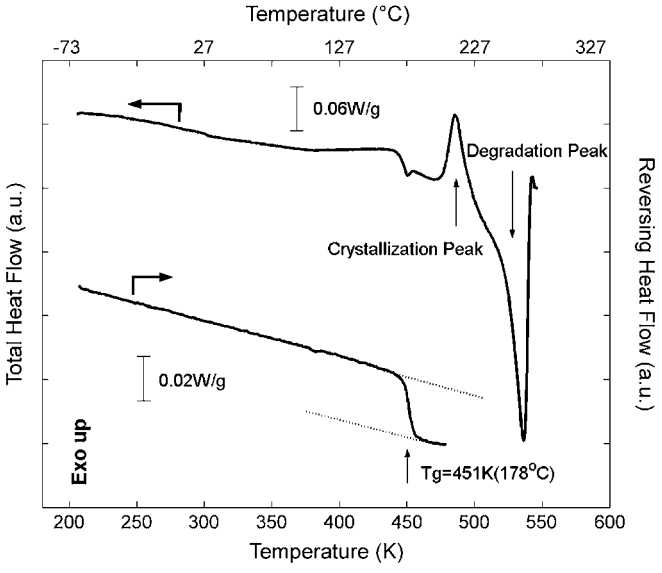

Fig. 2. TMDSC total heat flow (upper curve) and reversing heat flow (lower curve) vs. temperature of a less ordered, non-crystalline film from 213 to 548 K. The dotted lines are tangents from below and above the glass transition, used to determine the heat capacity increment at T_g.

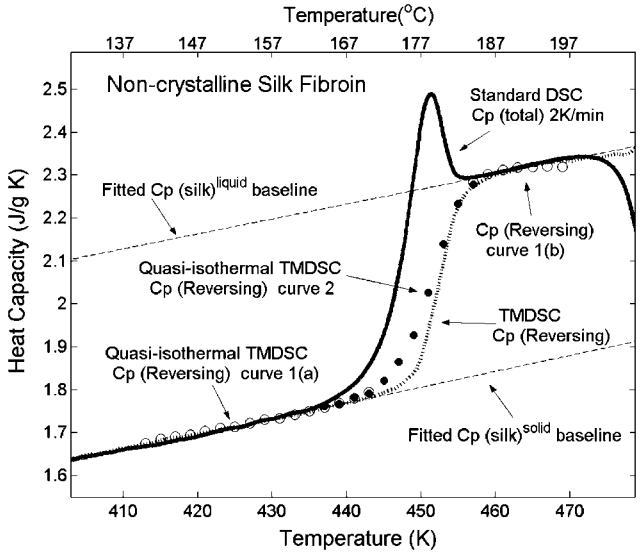

Fig. 3. Specific heat capacity curves from standard DSC (solid curve) and the specific reversing heat capacity curve from TMDSC (dotted curve) in a temperature region of the glass transition. Two quasi-isothermal TMDSC traces (empty and filled circles) are also shown for the comparison. The dashed lines are the baselines fitted to the data and extrapolated from below and above T_g, reflecting the heat capacities of the solid and liquid states, respectively.

Fig. 3 shows the specific heat capacity curve from total standard a DSC run (solid curve) and the specific reversing heat capacity curve from the TMDSC scan (dotted curve) in a temperature region of the glass transition. Two quasi-isothermal TMDSC traces are also shown for the comparison, using empty and filled circles. Curve 1 (open circles, part a) was measured from 413 to 443 K every 2 K and then immediately the temperature was jumped to 457 K, and the quasi-isothermal scan continued from 457 to 469 K every 2 K (open circles, part b). The jump procedure was implemented to minimize the chance that the silk would become crystallized by beta-sheet formation (during the long quasi-isothermal process), which can occur even for a temperature close to the glass transition. During the glass transition process, the mobility of silk fibroin chain has started to increase. Therefore, to avoid the effect of possible crystallization during long annealing in the glass transition region (20 min per holding temperature), a jump from the ending temperature of the solid state to the beginning temperature of the rubbery state was used to obtain the accurate liquid state heat capacity values at elevated temperature.

The three heat capacity traces in the solid state at temperatures below the glass transition are overlapped very well, no matter whether they are measured from standard DSC, reversing TMDSC, or quasi-isothermal TMDSC. In most of the temperature region of the liquid state, the liquid heat capacity obtained from these three methods also matched each other very well. However, as the temperature increases up to about 465 K, the heat capacity values from quasi-isothermal TMDSC scan begin to decrease gradually, due to the slight cold crystallization that can occur at these temperatures. For completeness, another quasi-isothermal TMDSC scan (filled circles) was performed in the temperature region of the glass transition with an increment of 2 K. These intermediate temperature data connect smoothly from the solid state to the liquid state quasi-isothermal data. In the standard DSC curve, an exothermic peak (not shown totally) due to the non-isothermal crystallization caused a decreasing process of the total heat capacity above 469 K.

In Fig. 3, two tangent lines are drawn with dashed lines. The tangent from below T_g gives the solid heat capacity $C_p^{\text{silk}}(T)^{\text{solid}}$, which is dominated by vibrational modes. Below T_g of the non-crystalline sample, we evaluated the specific heat capacity of the solid state and found $C_p^{\text{silk}}(T)^{\text{solid}} = 0.134 + 3.696 \times 10^{-3}T$(J/(g K)) with a correlation coefficient of 0.9931 (from 213 to 441 K). This result is consistent with the data we obtained by averaging three runs from the 310 to 440 K in our previous work [10]. The accuracy of the heat capacity is 3% in this study. The tangent above T_g gives the liquid state heat capacity $C_p^{\text{silk}}(T)^{\text{liquid}}$ for the less ordered non-crystalline sample.

According to the glass transition theory [20–29], in a semicrystalline polymer, three phases (mobile amorphous, rigid amorphous and immobilized crystal region) may be needed to describe the heat capacity increment occurring at the glass transition. However, our previous work has shown that silk fibroin is almost a purely two-phase material, comprising the mobile amorphous and immobilized crystal phases. Within the error limits on our measurement [10], we concluded that there is no rigid amorphous phase present in silk fibroin. Therefore, we can obtain $C_p^{\text{silk}}(T)^{\text{liquid}}$ directly from fitting our experimental data, and this is the only way to obtain $C_p^{\text{silk}}(T)^{\text{liquid}}$ because silk fibroin degrades at a temperature (536 K) lower than the crystal melting point. By averaging the three data sets from the different DSC methods (standard DSC, TMDSC and quasi-isothermal TMDSC), we find $C_p^{\text{silk}}(T)^{\text{liquid}} = 0.710 + 3.47 \times 10^{-3}T$ J/g K with an average correlation coefficient of 0.9986.

3.3. Glass transition of the silk–water system

The heat capacity study of the polymer and small molecules system has been well developed by Pyda [16,17]. Following his work, the heat capacity of the mixed system of amorphous polymer and small molecules is based on the evaluation of:

$$C_p(\text{poly–sm}) = C_{\text{vib}}(\text{poly–sm}) + C_{\text{conf}}(\text{poly–sm}) + C_{\text{ext}}(\text{poly–sm}) \quad (3)$$

where C_p (poly–sm) represents the total heat capacity at constant pressure for the system polymer/small molecules, C_{vib}(poly–sm) is the vibrational heat capacity at constant volume, C_{ext}(poly–sm) stands for the external heat capacity, and C_{conf}(poly–sm) denotes the conformational heat capacity. The major part of the total heat capacity comes from vibrational motion. The vibrational heat capacities of the polymer/small molecules system (first term on the right hand side of Eq. (3), can be estimated by the addition of C_p^{poly} (vib) and C_p^{sm}(vib) according to the equation:

$$C_{\text{vib}}(\text{poly–sm}) = X_{\text{poly}}C_p^{\text{poly}}(\text{vib}) + X_{\text{sm}}C_p^{\text{sm}}(\text{vib}) \quad (4)$$

where X_{poly} and X_{sm} are the molar fractions of polymer repeating units and small molecules, respectively [16,17]. If we normalize the specific heat capacity by weight unit, this equation can still be used by treating X_{poly} and X_{sm} as the weight fraction of polymer and small molecules.

The calculated mixed vibrational heat capacity for different component fractions, can serve as a baseline for the thermal analysis of the experimental mixed heat capacity. Silk–water system is a typical example of this model. Because silk fibroin is not a polymer with repeating monomer units, it is difficult to estimate the theoretical value of the C_p^{silk}(vib) by calculating the group and skeletal vibrational heat capacity contributions. Therefore, as a first approximation, the vibrational heat capacity of silk fibroin can be substituted with the experimental heat capacity of amorphous silk fibroin, as Wunderlich and co-workers have done on other polymer materials [30]. The $C_p^{\text{silk}}(T)^{\text{solid}}$ and $C_p^{\text{silk}}(T)^{\text{liquid}}$ for pure silk fibroin have been measured in the previous section. The vibrational heat capacity of the glassy water has been calculated by Pyda in his study of the starch–water system [16,17]. Therefore, the best fitting trace of the $C_p^{\text{water}}(T)^{\text{glassy}}$ for the temperature region we are interested in, 200–500 K, can be obtained. The liquid heat capacity of water was calculated by Seki and co-workers [31], and was found approximately to be $C_p^{\text{water}}(T)^{\text{liquid}} = 4.4083 + 4.35 \times 10^{-4}T$ J/g K. Therefore, to a first approximation, we can simply predict the total heat capacity of the silk–water system using:

$$C_p^{\text{silk–water}}(T)^{\text{solid}} = X_{\text{silk}}C_p^{\text{silk}}(T)^{\text{solid}} + X_{\text{water}}C_p^{\text{water}}(T)^{\text{glassy}} \quad (5a)$$

$$C_p^{\text{silk–water}}(T)^{\text{liquid}} = X_{\text{silk}}C_p^{\text{silk}}(T)^{\text{liquid}} + X_{\text{water}}C_p^{\text{water}}(T)^{\text{liquid}} \quad (5b)$$

where $C_p^{\text{silk–water}}(T)$ is the calculated specific heat capacity of the total silk–water system, $C_p^{\text{silk}}(T)$ and $C_p^{\text{water}}(T)$ the experimental specific heat capacities of silk and water, respectively, X_{silk} the weight fraction of silk in the system and X_{water} is the weight fraction of water, and they have the relation: $X_{\text{silk}} = 1 - X_{\text{water}}$.

In our study, we focused on the interaction of the solid silk film with the intermolecular bound water molecules. If intermolecular water evaporated from the film, we do not treat these water vapor molecules as part of silk–water system. Our results show that during the quick heating, the intermolecular water

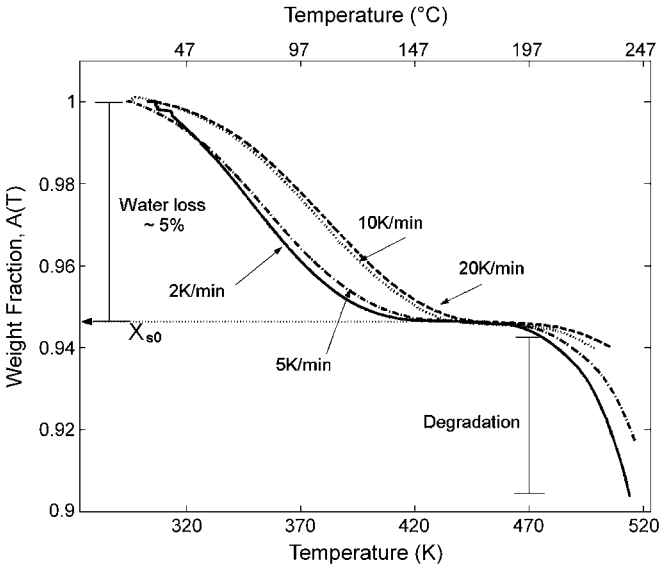

Fig. 4. TGA weight fraction, $A(T)$, vs. temperature of the silk film at heating rates of 2, 5, 10, and 20 K/min. The region of water loss and degradation are marked.

evaporates from the silk film into the air continuously. We can quantitatively assess the amount of water in the silk film using TGA. Fig. 4 shows TGA weight loss versus temperature of the silk film. The sample was sealed in a normal DSC pan and the empty pan was used to reset the zero point of the total weight. The heating rate for TGA is 5 K/min, the same as for the DSC scans. This figure shows that the silk film will start to release the water molecules into air at the temperature of about $T = 308$ K. As the temperature increases, more and more water evaporates and the total weight of silk film decreases until about 433 K. Above 433 K, there is no more intermolecular water in the film and the film became pure silk fibroin. Based on these results, and confirming the results of Fig. 1, the weight of the film will not change if we anneal the sample at 438 K to remove all the water.

To determine whether the evaporation rate of the intermolecular water varies with heating rate, silk films were also heated at rates of 2, 10, and 20 K/min. The data in Fig. 4 show that sample weight decrease is pushed to higher temperature as heating rate increases. However, the evaporation of water will come to an end at a temperature around 433 K. This result also demonstrates that when the silk film was quickly heated up to 438 K (e.g., at 20 K/min), the water will also be removed completely, and the film becomes pure silk fibroin. The total weight change of the film is around 5% independent of the heating rate.

To calculate the heat capacities of the silk–water system used in Eq. (5), we use the TGA data at 5 K/min. to form a temperature related function, $A(T)$, in the range of temperatures from 308–438 K. Below 308 K, the value of $A(T)$ is simply set to unity. First, we set the real time total mass of the silk–water system to be $M(T)$, and the initial total mass silk–water system to be M_0. Then we have: $A(T) = M(T)/M_0$. The initial weight fraction of the silk (X_{s_0}) in the silk–water system should equal the ratio of the unchangeable mass of pure silk fibroin to the total initial mass, which is $X_{s_0} = M_s/M_0$. Thus, the real time weight fraction of the silk can be derived from:

$$X_s = \frac{M_s}{M} = \frac{M_0 X_{s_0}}{M_0 A(T)} = \frac{X_{s_0}}{A(T)} \tag{6}$$

The weight fraction of the water (X_w) is simply written as $X_w = 1 - X_s$. We can now rewrite Eq. (5) for both solid and liquid heat capacities as:

$$C_p^{\text{silk-water}}(T) = \frac{X_{s_0}}{A(T)} C_p^{\text{silk}}(T) + \left(1 - \frac{X_{s_0}}{A(T)}\right) C_p^{\text{water}}(T) \tag{7}$$

The X_{s_0} can be simply obtained by measuring the TGA weight fraction from the end of weight loss (at $T \sim 433$ K), which is normally close to 95%. Since the total mass is always decreasing during the heating process, the measured heat capacity, c_{p_m}, should be corrected by the factor $A(T)$ from the beginning temperature of water loss (i.e., at 433 K). The corrected specific heat capacity c_{p_m}, satisfies:

$$c_{p_m} = \frac{C_p}{M} = \frac{C_p}{M_0 A(T)} = \frac{c_{p_0}}{A(T)} \tag{8}$$

Fig. 5 shows the reversing specific heat capacity from a typical rapid TMDSC heating scan at 5 K/min for silk fibroin film that contained intermolecular bound water (heavy curve). The corrected heat capacity of the silk–water system is shown for the sample with an initial silk fibroin weight fraction, $X_{s_0} = 0.9475$. The solid-state heat capacity baseline (solid line) was drawn according to the corrected Eq. (7), and for comparison, the solid and liquid state baselines of the pure silk without water are also shown (solid lines). For the total solid specific heat capacity, $C_p^{\text{silk-water}}(T)^{\text{solid}}$ good agreement exists in the low-

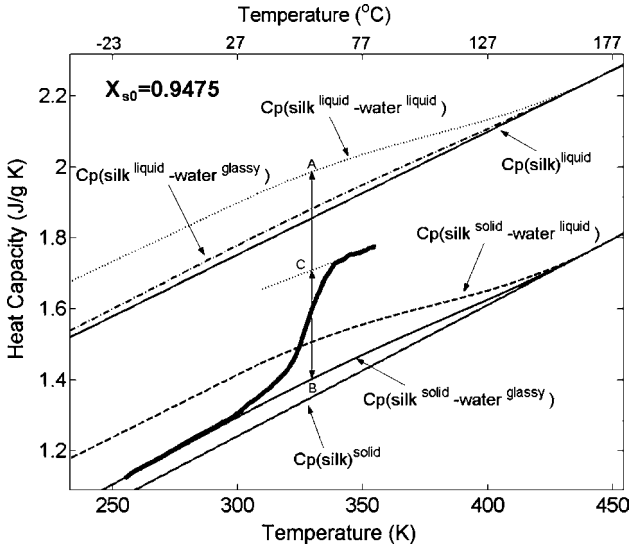

Fig. 5. Specific heat capacity vs. temperature for a silk film containing initially 0.0525 weight fraction of bounded water (heavy curve). The water-induces a low-temperature glass transition with mid-point indicated by the line BC. Solid lines represent the expected baseline heat capacities for silk solid, silk solid and glassy water, and silk liquid, as marked. The expected baselines for solid silk and liquid water (dashed line), liquid silk and liquid water (dotted line), and liquid silk and glassy water (dash-dotted line) are also shown. All the baselines were calculated using Eq. (7), correcting the weight fraction of water according to the function $A(T)$.

temperature region below about 240 K, indicating that only vibrational motions of silk and glassy water contribute to the heat capacity in this temperature region. Fig. 5 shows that water will induce a low-temperature glass transition at about 320 K (60 °C) for this silk fibroin film. The experimental heat capacity increases from the baseline of the solid-state silk–water system until a jump occurs at $T_g = 320$ K (60 °C). This is followed at higher temperature by an increase in the heat capacity that is parallel to that expected for the liquid $C_p^{\text{silk-water}}(T)^{\text{liquid}}$ (dotted line) and it occurs at a lower level. The expected change in the heat capacity at $T = 320$ K was estimated to be 0.5734 J/g K for the full step A to B, compared to the experimental heat capacity step B to C, which is only 0.2845 J/g K. The heat capacity increment at the water-induced T_g is also much smaller than that from the completely dried silk fibroin which occurs at $T_g = 451$ K. The above results are due to the assumption that silk fibroin chains and their intermolecular bound water are treated in total as a polymer–water system, and this system can gain the mobility and experience the transition to the rubbery state uniquely. In the glassy state, all water molecules participate in four hydrogen bonds (two as donor and two as acceptor) with the silk fibroin chains and are held relatively static. As water is heated, the increased thermal energy of water causes the hydrogen bonds to break. In this way, the intermolecular bound water molecules that remain in the film provide additional free volume for the polymer chains to experience a (lowered) glass transition.

To determine whether there will be a possible "cold" crystallization region just after this newly induced glass transition we performed the following test. When the film passed through the water-induced glass transition temperature (around 333 K) after quick heating, we annealed the sample for 4 h at a temperature $T = 433$ K, which is below the T_g of pure silk fibroin (451 K) but well above the water-induced T_g. The silk fibroin film was then taken out from the DSC pan and examined by X-ray scattering (data not shown). No beta-sheet crystals were found in this treated sample, which means this water-induced glass transition did not give the silk fibroin sample enough mobility to form the stacked intermolecular beta-sheet crystals.

For comparison, we can also consider two extreme situations: (1) if only the initially solid-state silk fibroin gained the mobility for transferring to the rubbery liquid state, and the intermolecular bound water molecules remaining in their glassy state. In this way, we can draw a baseline combining the heat capacities of liquid silk and glassy water (dash–dotted line) by Eq. (7). In Fig. 5, the measured data fall below the upper baseline derived by combining the heat capacities of liquid silk and glassy water, which means this lower glass transition cannot come from the heat capacity increment caused by the transition of solid silk fibroin to its liquid state while keeping the water molecules stable in their glassy state; (2) it might also be possible that initially only the glassy bound water broke some of its hydrogen bonds and transferred from the glassy state to the liquid state. This will give an upper baseline derived by combining the heat capacities of solid silk and liquid water (dashed line). We see that this combined heat-capacity baseline is much lower than the real experimental heat capacity data of the silk–water system at temperatures above the induced glass transition. This result indicates that the silk–water system can gain enough energy to let the intermolecular bound glassy water break some hydrogen bonds and transfer to liquid water.

Therefore, the mobility of the silk fibroin chain has been changed after the water-induced glass transition. Silk fibroin might form a new tighter tertiary structure after the loss of intermolecular bound water, a result that is confirmed by infrared spectral analysis and will be published separately.

4. Conclusion

Silk fibroin films cast from water solution contain bound water even after samples are dried in a vacuum oven. To remove the bound water, heat treatment at elevated temperatures is required. TGA results allow the water loss to be monitored quantitatively. The process of removing water and avoiding the induced glass transition is described in detail. The solid and liquid heat capacities of the pure dry silk fibroin were then obtained over the temperature region from 200 to 450 K.

When the combined silk–water system is studied, a water-induced lower glass transition is observed. Separate tests show that this glass transition does not give the silk mobility to form beta-sheets crystals. Calculation of the heat capacity baselines was made after correction for the temperature dependent water removal process. Comparison of the measured heat capacity of the silk–water system to the calculated baselines was made above the water-induced glass transition. Results show that the water-induced glass transition cannot arise simply from the phase transition of solid silk and glassy water to solid silk and liquid water. Although we cannot exclude the possibility that some bound glassy water become liquid, the principal contribution to the observed glass transition is from the solid silk to liquid silk transition. As temperature increases above the lower glass transition, all bound water eventually leaves the silk, and the free volume and the silk mobility are reduced. This allows the upper glass transition of the dried silk to be observed.

Acknowledgement

The authors thank the National Science Foundation Division of Materials Research, Polymers Program, for support of this research through grant DMR-0402849.

References

[1] Silk polymers: materials science and biotechnology, in: D.L. Kaplan, W.W. Adams, B. Farmer, C. Viney (Eds.), ACS Symposium Series 544, American Chemical Society, Washington, DC, 1994.
[2] K. McGrath, D. Kaplan (Eds.), Protein-Based Materials, Birkhauser Press, Boston, 1996, pp. 103–133.
[3] G.H. Altman, F. Diaz, C. Jakuba, T. Calabro, R.L. Horan, J.S. Chen, H. Lu, J. Richmond, D.L. Kaplan, Biomaterials 24 (2003) 401–416.
[4] C.W.P. Foo, D.L. Kaplan, Adv. Drug Deliv. Rev. 54 (2002) 1131–1143.
[5] M. Ishida, T. Asakura, M. Yokoi, H. Saito, Macromolecules 23 (1990) 88–94.
[6] X. Chen, D.P. Knight, Z.Z. Shao, F. Vollrath, Polymer 42 (2001) 9969–9974.
[7] A. Motta, L. Fambri, C. Migliaresi, Macromol. Chem. Phys. 203 (2002) 1658–1665.

[8] N. Agarwal, D.A. Hoagland, R.J. Farris, J. Appl. Polym. Sci. 63 (1997) 401–410.
[9] O.N. Tretinnikov, Y. Tamada, Langmuir 17 (2001) 7406–7413.
[10] X. Hu, D. Kaplan, P. Cebe, Macromolecules 39 (2006) 6161–6170.
[11] X. Hu, P. Cebe, Am. Chem. Soc. Div. Polym. Mater.: Sci. Eng. Prepr. 93 (2005) 652–653.
[12] R.M. Hodge, T.J. Bastow, G.H. Edward, G.P. Simon, A.J. Hill, Macromolecules 29 (1996) 8137–8143.
[13] Y.S. Kim, L.M. Dong, M.A. Hickner, T.E. Glass, V. Webb, J.E. McGrath, Macromolecules 36 (2003) 6281–6285.
[14] K.Y. Lee, W.S. Ha, Polymer 40 (1999) 4131–4134.
[15] H.J. Jin, D.L. Kaplan, Nature 424 (2003) 1057–1061.
[16] M. Pyda, J. Polym. Sci. Part B Polym. Phys. 39 (2001) 3038–3054.
[17] M. Pyda, Macromolecules 35 (2002) 4009–4016.
[18] M. Pyda, B. Wunderlich, Macromolecules 32 (1999) 2044–2050.
[19] K. Ishikiriyama, B. Wunderlich, J. Therm. Anal. 50 (1997) 337–346.
[20] H. Xu, P. Cebe, Macromolecules 37 (2004) 2797–2806.
[21] H. Xu, P. Cebe, Macromolecules 38 (2005) 770–779.
[22] B. Wunderlich, Y.M. Jin, A. Boller, Thermochim. Acta 238 (1994) 277–293.
[23] B. Wunderlich, Macromolecular Physics: Crystal Nucleation, Growth, Annealing, vol. 2, Academic Press, New York, 1976, p. 141.
[24] A. Boller, I. Okazaki, K. Ishikiriyama, G. Zhang, B. Wunderlich, J. Therm. Anal. 49 (1997) 1081–1088.
[25] M. Pyda, A. Boller, J. Grebowicz, H. Chuah, B.V. Lebedev, B. Wunderlich, J. Polym. Sci. Part B Polym. Phys. 36 (1998) 2499–2511.
[26] J. Grebowicz, S.F. Lau, B. Wunderlich, J. Polym. Sci. Polym. Symp. (1984) 19–37.
[27] H. Suzuki, J. Grebowicz, B. Wunderlich, Makromolekulare Chemie-Macromol. Chem. Phys. 186 (1985) 1109–1119.
[28] P. Huo, P. Cebe, Colloid Polym. Sci. 270 (1992) 840–852.
[29] P.T. Huo, P. Cebe, Macromolecules 25 (1992) 902–909.
[30] U. Gaur, M.Y. Cao, R. Pan, B. Wunderlich, J. Therm. Anal. 31 (1986) 421–445.
[31] M. Sugisaki, H. Suga, S. Seki, Bull. Chem. Soc. Jpn. 41 (1968) 2591.